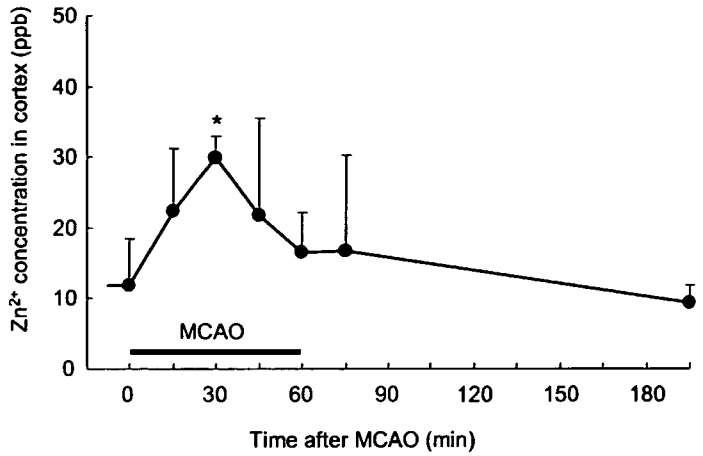

Fig. 7 Extracellular Zn^{2+} levels in the cortex during MCAO.
Data are expressed as the mean ± S.D. *p < 0.05 for significantly different from the pre-ischemic level (Dunnett's test).

course is consistent with that of glutamate. At the peak, the extracellular zinc concentration was about twice the basal level, in contrast with the amount of glutamate which increased about 50 fold. These results suggest that, the concentration of zinc released during MCAO could not reach a toxic level. In this model, intracerebroventricular (i.c.v.) injection of Ca-EDTA 30 min prior to occlusion, accelerated the increase of infarction volume (Fig. 8). N-(6-methoxy-8-quinolyl)-p-toluenesulfonamide (TSQ) staining revealed that there no zinc accumulated in the infarcted area or at its boundary. These results suggest that, in the rat MCAO model, the zinc released from synaptic vesicles may provide protection against ischemic neuronal injury. These results suggest that the effect of zinc on ischemic neuronal death differs depending on the ischemic region or severity.

2.2.2. Development of a highly membrane permeable zinc complex providing protection against ischemic neuronal injury

As shown in 2.2.1, Zn^{2+} blocks NMDA-induced depolarizing currents and protects cultured cortical neurons from the NMDA receptor-mediated neurotoxicity of glutamate. The results suggested the potential usefulness of zinc for the prevention of ischemic neuronal damage in the brain.

The basic requirements for therapeutic drugs to effectively prevent ischemic neuronal damage in the brain include high membrane permeability resulting in a rapid and significant uptake in the brain and protective action against glutamate's toxicity. However, Zn^{2+} does not readily permeate the blood brain barrier due to its high polarity [29]. Thus, a zinc compound that can cross cell

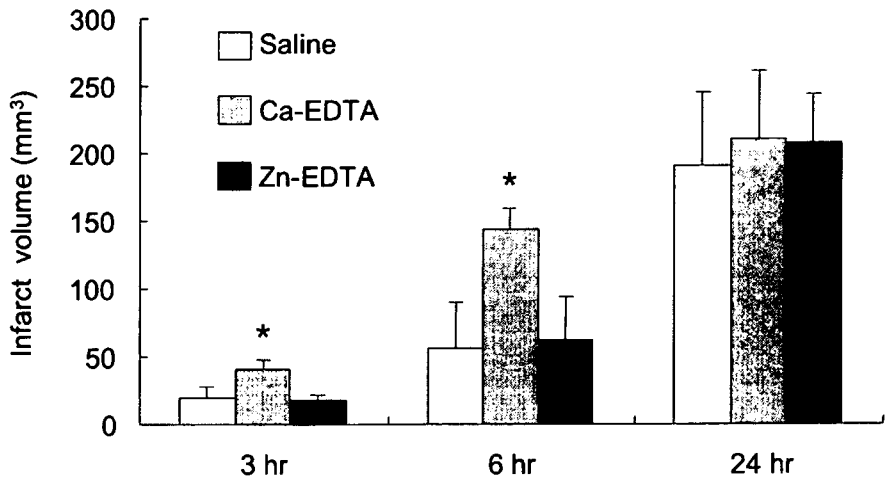

Fig. 8 Effect of Ca- and Zn-EDTA on the development of infarcted areas after MCAO.
Data are expressed as means ± S.D. (n= 3- 5). *P< 0.01 for significantly different from the saline-treated group (Dunnett's test).

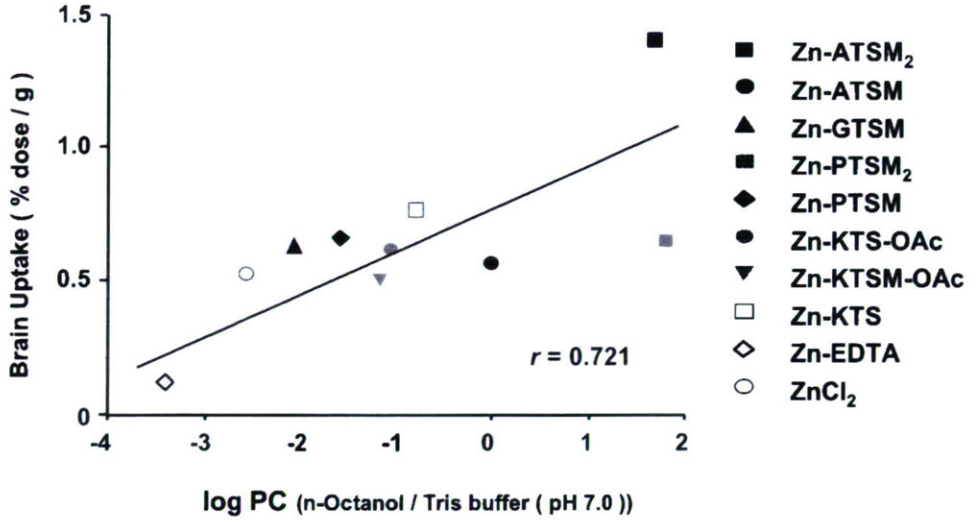

Fig. 9 Relationship between uptake in the brain and the octanol : Tris buffer (pH 7.0) partition coefficient (log P) for ^{65} Zn-BTS complexes.
Uptake was expressed as % dose/ g of tissue at 1 h post-injection of radiolabeled compounds into mice.

membranes and provide protection against NMDA receptor-mediated glutamate neurotoxicity, would seem to be a therapeutic drug for the prevention of ischemic neuronal damage.

Our previous studies demonstrated that bis(thiosemicarbazone) (BTS) derivatives formed stable chelates with divalent cations like copper and zinc ions, and that certain BTS complexes of Cu^{2+} were readily distributed in cerebral tissues because of greater membrane permeability [30-34]. Thus, we synthesized several Zn-BTS chelates and assessed their biodistribution, especially their uptake into the brain. It was found that the uptake basically increased along with the lipophilicity of the compound and, among the zinc complexes tested, the 2,3 -butanedione bis(N-dimethylthiosemicarbazonato) zinc complex (Zn-$ATSM_2$) displayed the highest cerebral level, 2.7-fold that of Zn^{2+} at 1 h post-injection (Fig. 9) [31]. No adverse effect on behavior was observed after the administration of these zinc compounds [35].

The protective effect of Zn-$ATSM_2$ on the neurotoxicity of glutamate was examined in cultured retinal neurons and compared with that of Zn^{2+} because the retina is rich in glutamatergic neurons [36]. Glutamate treatment markedly reduced cell viability and the addition of Zn^{2+} markedly reversed this tendency. Zn-$ATSM_2$ provided protection against this neurotoxicity and the effect was similar to that of Zn^{2+}, whereas the ligand, $ATSM_2$, did not affect cell viability (Fig 10) [37].

Furthermore, we examined the effects in vivo of systemically administered Zn-$ATSM_2$ on ischemic neuronal injury using the rodent model. Compared with the control group, the infarct volume in the Zn-$ATSM_2$-treated groups 30min before the onset of occlusion and immediately after reperfusion, was significantly reduced. Furthermore, no morphological or physiological alterations were observed after the injection of Zn-$ATSM_2$. Thus, Zn

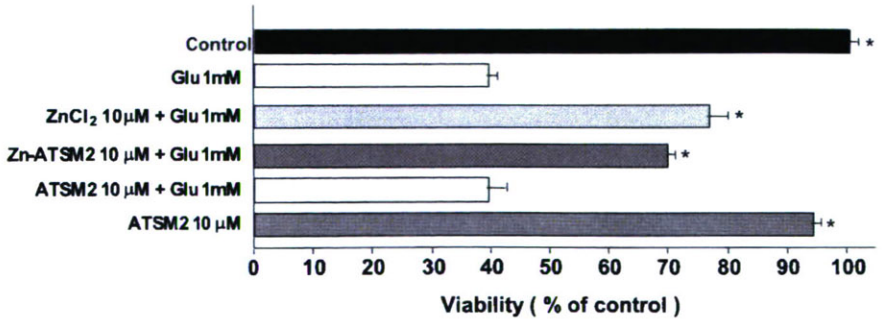

Fig. 10 The effects of Zn-$ATSM_2$, Zn^{2+} on glutamate-induced retinal neurotoxicity.
Neurotoxicity was induced by 1 mM glutamate (Glu). *P < 0.05 vs. Group treated with glutamate (Student's t-test). Values are the mean ± SEM. (n = 5).

-ATSM$_2$ with good ability to permeate the blood-brain barrier, had protective effects on the brain when systemically administered early in a model of temporary focal ischemia.

References

1) Saji H : Targeted Delivery of Radiolabeled Imaging and Therapeutic Agents : Bifunctional Radiopharmaceuticals. Critical Reviews in Therapeutic Drug Carrier Systems. 16 : 209-244, 1999.
2) Verbruggen AM : Bifunctional chelators for technetium-99m. Mather SJ (ed) : Current Directions in Radiopharmaceutical Research and Development. Kluwer Academic Publishers, Dordrecht, 1996, pp 31-46..
3) Dilworth JR and Parrott SJ : Radiopharmaceutically relevant chemistry of technetium and rhenium. Mather SJ (ed) : Current Directions in Radiopharmaceutical Research and Development. Kluwer Academic Publishers, Dordrecht, 1996, pp 1-29.
4) Holman BL, Hellman RS, Goldsmith SJ, Mena IG., Leveille J, Gerundidi Gherrardi P, Moretti JL, Bischof-Delaloye A, Hill TC and Rigo PM : Biodistribution, dosimetry, and clinical evaluation of technetium-99m ethyl cysteinate dimer in normal subjects and in patients with chronic cerebral infarction. J Nucl Med, 30 : 1018-1024, 1989.
5) Walovitch RC, Hill TC, Garrity ST, Cheesman EH, Burgess BA, OLeary DH, Watson AD, Ganey MV, Morgan RA and Williams SJ : Characterization of technetium-99m-L,L-ECD for brain perfusion imaging, Part 1 : pharmacology of techetium-99m ECD in nonhuman primates. J Nucl Med, 30 : 1892-1901, 1989.
6) Leveille J, Demonceau G., De Roo M, Rigo P, Tailefer R, Morgan RA, Kupranick D and Walovitch RC : Characterization of technetium-99 m-L,L-ECD for brain perfusion imaging, Part 2 : biodistribution and brain imaging in humans, J Nucl Med, 30 : 1902-1910, 1989.
7) Horiuchi KS and Yokoyama A : Radioactive metal complexes used for tumor diagnosis. Berthon G. (ed) : Handbook of Metal-Ligand Interactions in Biological Fluids. Mercel Dekker, New York, 1995, pp 1052-1066.
8) Jurisson S, Berning D, Jia W and Ma D : Coordination compounds in nuclear medicine. Chem Rev, 93 : 1137-1156, 1993.
9) Fischman AJ, Badich JW and Strauss HW : A ticket to ride ; peptide radiopharmaceuticals. J Nucl Med, 34 : 2253-2263, 1993.
10) Hom RK, and Katzenellenbogen JA : Technetium-99m-labeled receptor-specific small-molecule radiopharmaceuticals : recent developments and encouraging results. Nucl Med Biol, 24 : 485-498, 1997.
11) Portenoy RK, Lesage P : Management of cancer pain. Lancet. 353 : 1695-1700, 1999.
12) Lewington VJ : Bone-seeking radionuclides for therapy. J Nucl Med 46 : Suppl 1 : 38S-47S, 2005.
13) Lam MG, de Klerk JM, van Rijk PP : ^{186}Re-HEDP for metastatic bone pain in breast cancer patients. Eur J Nucl Med Mol Imaging 31 : Suppl 1 : S162-170, 2004.
14) de Klerk JM, van Dijk A, van het Schip AD, Zonnenberg BA, van Rijk PP : Pharmacokinetics of rhenium-186 after administration of rhenium-186-HEDP to patients with bone metastases. J Nucl Med 33 : 646-651, 1992.
15) de Winter F, Brans B, Van De Wiele C, Dierckx RA. : Visualization of the stomach on rhenium-186 HEDP imaging after therapy for metastasized prostate carcinoma. Clin Nucl Med. 24 : 898-899, 1999.
16) Ogawa K, Mukai T, Arano Y, Hanaoka H, Hashimoto K, Nishimura H, and Saji H. : Design of a radiopharmaceutical for the palliation of painful bone metastases : rhenium-186-labeled bisphosphonate derivative. J Labelled Cmp Radiopharm 47 : 753-761, 2004.
17) Fleisch H : Bisphosphonates : mechanisms of action.. Endocr Rev 19 : 80-100, 1998.
18) van Beek E, Hoekstra M, van de Ruit M, Lowik C, Papapoulos S : Structural requirements for bisphosphonate actions in vitro. J Bone Miner Res 9 : 1875-1882, 1994.
19) Ogawa K, Mukai T, Arano Y, Otka A, Ueda M, Uehara T, Magata Y, Hashimoto K and Saji H : Rhemium-186-monoaminemonoamidedithiols conjugated bisphosphonate derivatives for bone pain palliation. Nucl Med Biol 33 : 513-520, 2006.
20) Ogawa K, Mukai T, Arano Y, Ono M, Hanaoka H, Ishino S, Hashimoto H, Nishimura H and Saji H : Development of a rhenium-186-labeled MAG3-conjugated bisphosphonate for the palliation of metastatic bone pain based on the concept of bifunctional radiopharmaceuticals. Bioconjug Chem 16 : 751-757, 2005.
21) Frederickson CJ : Neurobiology of zinc and zinc-containing neurons. Int Rev Neurobiol 31 : 145-238,

1989.

22) Ueno S, Tsukamoto M, Hirano T, Kikuchi K, Yamada MK, Nishiyama N, Nagano T, Matsuki N and Ikegaya Y : Mossy fiber Zn^{2+} spillover modulates heterosynaptic N-methyl-D-aspartate receptor activity in hippocampal CA3 circuits. J Cell Biol **158** : 215-220, Epub 2002 Jul 2015, 2002.

23) Howell GA, Welch MG. and Frederickson CJ : Stimulation-induced uptake and release of zinc in hippocampal slices. Nature **308** : 736-738, 1984.

24) Smart TG, Xie X and Krishek BJ : Modulation of inhibitory and excitatory amino acid receptor ion channels by zinc. Prog Neurobiol **42** : 393-341, 1994.

25) Koh JY, Suh SW, Gwag BJ, He YY, Hsu CY and Choi DW : The role of zinc in selective neuronal death after transient global cerebral ischemia. Science **272** : 1013-1016, 1996.

26) Kitamura Y, Iida Y, Abe J, Ueda M, Mifune M, Kasuya F, Ohta M, Igarashi K, Saito Y and Saji H : Protective effect of zinc against ischemic neuronal injury in a middle cerebral artery occlusion model. J Pharmacol Sci **100** : 142-148, 2006.

27) Kitamura Y, Iida Y, Abe J, Mifune M, Kasuya F, Ohta M, Igarashi K, Saito Y and Saji H : In vivo measurement of presynaptic Zn2+ release during forebrain ischemia in rats. Biol Pharm Bull **29** : 821-823, 2006.

28) Kitamura Y, Iida Y, Abe J, Mifune M, Kasuya F, Ohta M, Igarashi K, Saito Y and Saji H : Release of vesicular Zn(2+) in a rat transient middle cerebral artery occlusion model. Brain Res Bull **69** : 622-625, 2006.

29) Peynolds IJ and Miller RJ : [^{3}H]MK801 binding to the NMDA receptor / ionophore complex is regulated by divalent cations : evidence for multiple regulatory sites. Eur J Pharmacol 151 : 103-112, 1988.

30) Gingras BA, Suprunchuk T and Bayley CH : The preparation of some thiosemicarbazones and their copper complexes. Can J Chem 40 : 1053-1059, 1962.

31) Green MA, Kippenstein DL and Tennison JR : Copper(II) bis(thiosemicarbazone) complexes as potential tracers for evaluation of cerebral and myocardial blood flow with PET. J Nucl Med 29 : 1549-1557, 1988.

32) John EK and Green MA : Structure-activity relationships for metal-labeled blood flow tracers : comparison of keto aldehyde bis(thisemocarbazonato)copper(II) derivatives. J Med Chem 33 : 1764-1770, 1990.

33) Saji H, Saiga A, Iida Y, Magata Y and Yokoyama A : Synthesis and in vivo behavior of a copper-64-labeled dithiosemicarbazone derivative coupled to a dihydropyridine carrier. J Label Comp Radiopharm 33 : 127-135, 1993.

34) Wada K, Fujibayashi Y and Yokoyama A : Copper (II) [2,3-butanedionebis (N^4-methylthiosemicarbazone)], a stable superoxide dismutase-like copper complex with high membrane penetrability. Arch Biochem Biophys 310 : 1-5, 1994.

35) Saji H, Kinoshita T, Kubota M, Kaneda K, Akaike A, Kikuchi M, Kashii S, Honda Y, Iida Y, Magata Y, Yokoyama A. Brain permeable zinc complex with neuroprotective action. s.t.p. Pharma Sci 7 : 92 -97, 1997.

36) Karcioglu ZA : Zinc in the eye. Surv Ophthalmol 27 : 114-122, 1982.

37) Kubota M, Iida Y, Magata Y, Kitamura Y, Kawashima H, Saji H : Mechanisom of [2,3-butanedione bis(N^4-dimethylthiosemicarbazone)zinc (Zn-ATSM2)-induced protection of cultured hippocampal neurons against N-methyl-d-asparatate receptor-mediated glutamate cytotoxicity. Jan J Pharmaco 84 : 334-338, 2000.

Eur J Nucl Med Mol Imaging (2007) 34:2096–2105
DOI 10.1007/s00259-007-0529-8

ORIGINAL ARTICLE

Extensive FDG uptake and its modification with corticosteroid in a granuloma rat model: an experimental study for differentiating granuloma from tumors

Songji Zhao · Yuji Kuge · Masashi Kohanawa · Toshiyuki Takahashi · Hidekazu Kawashima · Takashi Temma · Toshiki Takei · Yan Zhao · Koh-ichi Seki · Nagara Tamaki

Received: 6 July 2006 / Accepted: 3 July 2007 / Published online: 1 September 2007

Abstract
Introduction Increased ^{18}F-fluorodeoxyglucose (FDG) uptake in inflammatory lesions, particularly in granulomatous inflammation (e.g., sarcoidosis), makes it difficult to differentiate malignant tumors from benign lesions and is the main source of false-positive FDG-PET findings in oncology. Here, we developed a rat granuloma model and examined FDG uptake in the granuloma. The effects of corticosteroid on FDG uptake in the granuloma were compared with those in a malignant tumor.

Methods Rats were inoculated with *Mycobacterium bovis* bacillus Calmette-Guérin (BCG) or allogenic hepatoma cells, and subdivided into control and pretreated (methylprednisolone acetate, 8 mg/kg i.m.) groups. Radioactivity in tissues was determined 1 h after the FDG injection. FDG-PET was performed in rats bearing BCG granulomas or tumors before and after prednisolone treatment.
Results Mature epithelioid cell granuloma-formation and massive lymphocyte-infiltration were observed in the control group of granuloma, histologically similar to sarcoidosis. The mean FDG uptake in the granuloma was comparable to that in the hepatoma. Prednisolone reduced epithelioid cell granuloma-formation and lymphocyte-infiltration. Prednisolone significantly decreased the level of FDG uptake in the granuloma (52% of control), but not in the hepatoma. The FDG uptake levels in the granulomas and tumors were clearly imaged with PET.
Conclusion We developed an intramuscular granuloma rat model that showed a high FDG uptake comparable to that of the tumor. The effect of prednisolone pretreatment on FDG uptake was greater in the granuloma than in the tumor. These results suggest that BCG-induced granuloma may be a valuable model and may provide a biological basis for FDG studies.

Keywords FDG · Granuloma · Tumor · Corticosteroid · Rat

S. Zhao · T. Takei · Y. Zhao · N. Tamaki (✉)
Department of Nuclear Medicine, Graduate School of Medicine, Hokkaido University,
Kita 15 Nishi 7, Kita-ku,
Sapporo 060-8638, Japan
e-mail: natamaki@med.hokudai.ac.jp

Y. Kuge
Department of Molecular Imaging, Graduate School of Medicine, Hokkaido University,
Sapporo, Japan

Y. Kuge · H. Kawashima · T. Temma
Department of Patho-functional Bioanalysis, Graduate School of Pharmaceutical Sciences, Kyoto University,
Kyoto, Japan

M. Kohanawa
Department of Microbiology, Graduate School of Medicine, Hokkaido University,
Sapporo, Japan

T. Takahashi
Department of Pathology, Hokkaido Gastroenterology Hospital,
Sapporo, Japan

K. Seki
Central Institute of Isotope Science, Hokkaido University,
Sapporo, Japan

Introduction

PET using FDG has become a very useful imaging tool not only for detecting and staging malignant tumors but also for monitoring therapy response and for differentiating malignant tumors from benign lesions [1]. These applications are

based on the increased FDG uptake due to enhanced glucose utilization in most tumors. Recent investigations, however, have shown that FDG accumulates not only in malignant tumors but also in various forms of inflammatory lesions, particularly in granulomatous lesions, such as sarcoidosis or active inflammatory processes after chemoradiotherapy [2–4]. Increased FDG uptake in such inflammatory lesions makes it difficult to differentiate malignant tumors from benign lesions and is the main source of false-positive FDG-PET findings in oncology [5]. Thus, it is of great importance to investigate FDG uptake in granulomatous lesions for accurately differentiating malignant and benign lesions by FDG-PET. However, FDG uptake in granulomatous lesions remains unclarified, mainly due to the lack of suitable animal models. To the best of our knowledge, there have been no studies of FDG uptake in experimental granulomatous lesions to date, although increased FDG uptake in inflammatory lesions has been reported in experimental inflammation induced by intramuscular injection of *Staphylococcus aureus* (*S. aureus*) or turpentine oil [5, 6]. Thus, we developed a granuloma rat model.

In the present study, we induced granuloma in the muscle of rats by BCG inoculation and examined FDG uptake in the granuloma in comparison with that in a tumor. In addition, we determined the effect of predonisolone pretreatment on FDG uptake in the granuloma to evaluate whether corticosteroid pretreatment facilitates the differentiation of malignant tumors from benign lesions by FDG -PET.

Materials and methods

Animal studies

All experimental protocols were approved by the Laboratory Animal Care and Use Committee of Hokkaido University. Eight-week-old male Wistar King Aptekman/hok (WKAH) rats (supplied by the Experimental Animal Institute, Graduate School of Medicine, Hokkaido University, Sapporo) were used in all experiments. The *Mycobacterium bovis* bacillus Calmette-Guérin (BCG), Japan strain, was grown on Middlebrook 7H11 agar (Difco Laboratories, Detroit, Mich), suspended in PBS with 0.05% Tween 20, and stocked at–80°C. A 1×10^7 CFU/rat dose of BCG, which was determined in our preliminary experiments, was inoculated into the left calf muscle of rats to induce appropriate sizes and numbers of granulomatous lesions. To produce an experimental tumor, rats were inoculated with a suspension of allogenic hepatoma cells (KDH-8, 1×10^6 cells/rat) into the left calf muscle [7]. Nineteen days after BCG inoculation or 14 days after KDH-8 inoculation, when the BCG-induced granulomatous lesions were 3–8 mm in diameter, or when the KDH-8-induced tumor tissues were 20–30 mm in diameter, the rats were fasted overnight and then randomly divided into two subgroups: prednisolone (PRE)-pretreated and control (untreated) (n=5–6, in each group). The sizes of the granuloma and tumors were checked under palpation, and then measured using calipers. The rats in the PRE-pretreated group were intramuscularly injected with methylprednisolone acetate (8 mg/kg body weight) in the left brachialis muscle 20 h before the FDG injection, according to the methods reported by Gemma et al. [8]. Each rat was anaesthetized with pentobarbital (50 mg/kg body weight, i.p.) and was injected in the tail vein with 5–6 MBq of FDG. The rats were kept under anaesthesia for the rest of the experiment. Sixty minutes after the FDG injection, the animals were sacrificed and tumor, granuloma tissues, and other organs were excised. The tissues and blood samples were weighed, and radioactivity was determined using a gamma counter (1480 WIZARDTM3″; Wallac Co., Ltd.). FDG uptake in the tissues was expressed as the percentage of injected dose per gram of tissue after being normalized to the animal's weight (%ID/g × kg). The lesion (granuloma or tumor)-to-muscle (L/M) ratio and the lesion (granuloma or tumor)-to-blood (L/B) ratio of FDG uptake were calculated from the (%ID/g)×kg value of each tissue [6]. By using tissue samples from the tumors and granulomas, frozen specimens and formalin-fixed, paraffin-embedded specimens were prepared for subsequent histologic staining. Blood samples for glucose measurement were obtained immediately before FDG injection and immediately before sacrifice. Blood glucose level was determined using a biochemical analyzer (MediSense, Dainobot Co., Ltd.).

Histochemical studies

Immunohistochemical staining for immune-associated antigen (Ia) was performed using a monoclonal antibody (mAb) (mouse IgG, MRC OX-6, Oxford Biotechnology Ltd.) that recognizes a monomorphic determinant of the rat Ia, MHC class II present on B lymphocytes, dendritic cells, some macrophages, and certain ephithelial cells. To further support the Ia-positive (Ia+) staining, other mAbs, namely, MRC OX-3 and MRC OX-17 were also used. The MRC OX-3 mAb (Serotec), a mouse anti-rat RT1Bu mAb, recognizes a polymorphic determinant of the rat Ia-A antigen RT1Bu (class II polymorphic) found on B cells, dendritic cells, and certain epithelial cells. The MRC OX-17 mAb (Serotec) recognizes a monomorphic determinant of the rat RT-1D (class II monomorphic), the rat homologue of the mouse Ia-E, which has a similar structure to the Ia-A antigen and reacts with anti-Ia alloantibodies. The MRC OX-17 mAb does not cross-react with the rat Ia-A (RT-1B) antigen, while both class II monomorphic MRC OX-6 and MRC OX-17 mAbs were active against determinants found in all rat strains. The different cell types were characterized

by positive staining with several monoclonal antibodies, i.e., RM-4 (Cosmo Bio Co., Ltd.) for macrophages, MRC OX-8 (mouse anti-rat CD8 alpha mAb, Serotec) for nonhelper T cells, and MRC OX-35 (mouse anti-rat CD4 mAb, Serotec) for helper T cells. The epithelioid cells and macrophages found around epithelioid cell granulomas were determined by positive staining with RM-4 (Fig. 2c). T cell subsets were characterized using MRC OX-35 and MRC OX-8.

The formalin-fixed, paraffin-embedded tumor and granuloma tissues were sectioned at 3 μm thickness and stained with hematoxylin and eosin (HE), whereas the frozen granuloma tissues were cut at 4 μm thickness. Immunohistochemical staining was carried out according to a standard immunostaining procedure [7–9]. Briefly, after deparaffization and rehydration (for MRC OX-6, MRC OX-8, and RM-4 mAbs), tissue sections were heated at 121°C for 15 min in 10 mM sodium citrate buffer, pH 6.0, for antigen retrieval (MRC OX-6 mAb). Frozen sections were fixed in ethanol (for MRC OX-3, MRC OX-17, and MRC OX-35 mAbs). Endogenous peroxidase activity was blocked for 5 min in methanol containing 3% hydrogen peroxide. Thereafter, slides were incubated with primary antibodies for 30 min at room temperature. The bound antibody was visualized by the avidin/biotin conjugate immunoperoxidase procedure using the HISTOFINE SAB 2 system HRP (Dako, Japan) and 3,3′-diaminobenzidine tetrahydrochloride (DAB) (Dako, Japan). Counterstaining was performed with hematoxylin.

PET imaging

PET experiments were performed in rats bearing BCG granulomas or KDH-8 tumors before (control) and after a prednisolone treatment. Eighteen days after BCG inoculation or 13 days after KDH-8 inoculation, the rats (n=3 for BCG granulomas and KDH-8 tumors, respectively) were fasted overnight, and anesthetized with pentobarbital (50 mg/kg body weight, i.p.). The rats were placed in a PET scanner (SHR-7700L, Hamamatsu Photonics, Hamamatsu, Japan) in a supine position and injected with FDG (28–30 MBq/rat) in the lateral tail vein. Sixty minutes after the injection of FDG, the rats underwent a first PET scanning for 15 min. After the PET scanning, the rats were treated with methylprednisolone acetate (8 mg/kg body weight). Twenty hours after the prednisolone treatment, a second FDG-PET scan was carried out using the same procedures as the first PET scan. The PET images were reconstructed by a standard filtered back-projection using a Hamming filter into a 256 × 256 × 31 (0.6 × 0.6 × 3.6 mm) matrix. The spatial resolution of the reconstructed images was 2.7 mm in the plane [10].

Statistical analysis

All values are expressed as mean ± standard deviation. To evaluate the significance of the differences in the values obtained between the control group and the treated group, an unpaired student's t test was performed.

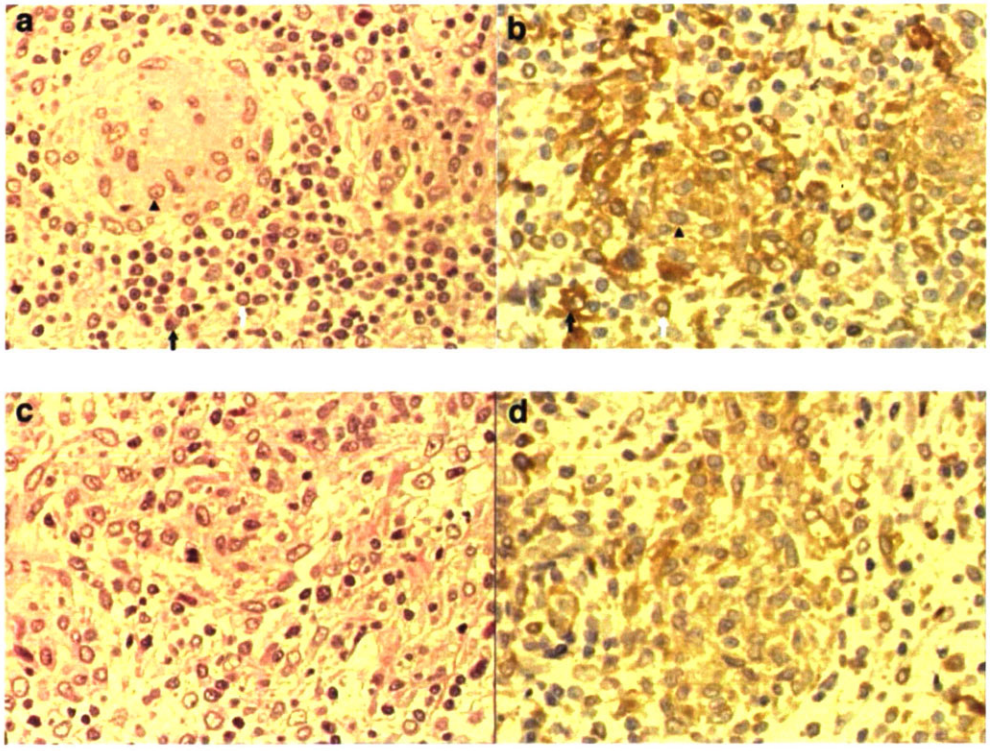

Fig. 1 Microscopic images (x 400) of HE-stained (**a**, **c**) and immunostained granuloma (**b**, **d**) for Ia antigen with MRC OX-6 mAb in control (**a**, **b**) and pretreated rats (**c**, **d**). **a** Mature epithelioid cell granuloma-formation and massive lymphocyte-infiltration. **b** Infiltrations of Ia-positive epithelioid cells and macrophages in granuloma and Ia-positive lymphocytes in granuloma periphery (for MRC OX-6). **c** Reduction of epithelioid cell granuloma-formation and lymphocyte-infiltration. **d** Reduction of infiltrations of Ia+ macrophages and Ia+ lymphocytes around granuloma. *Black arrow head* indicates epithelioid cell granuloma; *black arrow*, macrophage infiltration; *white arrow*, lymphocyte infiltration

A two-tailed value of $P<0.05$ was considered significant. The statistical program Stat View 5.0 was used for the data assessment.

Results

Histopathological findings

In the control animals inoculated with BCG, mature epithelioid cell granuloma-formation and massive lymphocyte-infiltration were observed in the calf muscle (Fig. 1a). Immunohistochemical staining with the MRC OX-6 mAb showed the accumulation of Ia^+ macrophages and Ia^+ lymphocytes into the periphery of the granuloma (Fig. 1b). In the prednisolone pretreatment group, reduction in the levels of epithelioid cell granuloma-formation and lymphocyte-infiltration and in the levels of Ia^+ macrophage-infiltration and Ia^+ lymphocyte-infiltration were observed (Fig. 1c and d). Immunostaining with MRC OX-3 and MRC OX-17 mAbs also showed the accumulation of Ia+ macrophages and Ia+ lymphocytes into the periphery of the granulomas in the control animals (Fig. 2a and b).

The different cell types in the granulomatous tissues were characterized by positive staining with several monoclonal antibodies. The epithelioid cells and macrophages determined by positive staining with RM-4 were found in the epithelioid cell granulomas and around epithelioid cell granulomas (Fig. 2c). Immunohistochemical staining of CD4 and CD8 showed numerous CD4+ (helper T cells) and CD8+ T cells (nonhelper T cells) surrounding the granulomas (Fig. 2d and e).

In the control animals inoculated with KDH-8, massive viable and proliferating cancer cells were observed by HE staining (Fig. 3a). Immunohistochemical staining with the MRC OX-6 mAb showed scattered Ia^+ macrophages-infiltration and Ia^+ lymphocytes-infiltration into the viable tumor cells (Fig. 3b). There were no histopathological changes for tumor tissue after treatment with prednisolone (Fig. 3c and d).

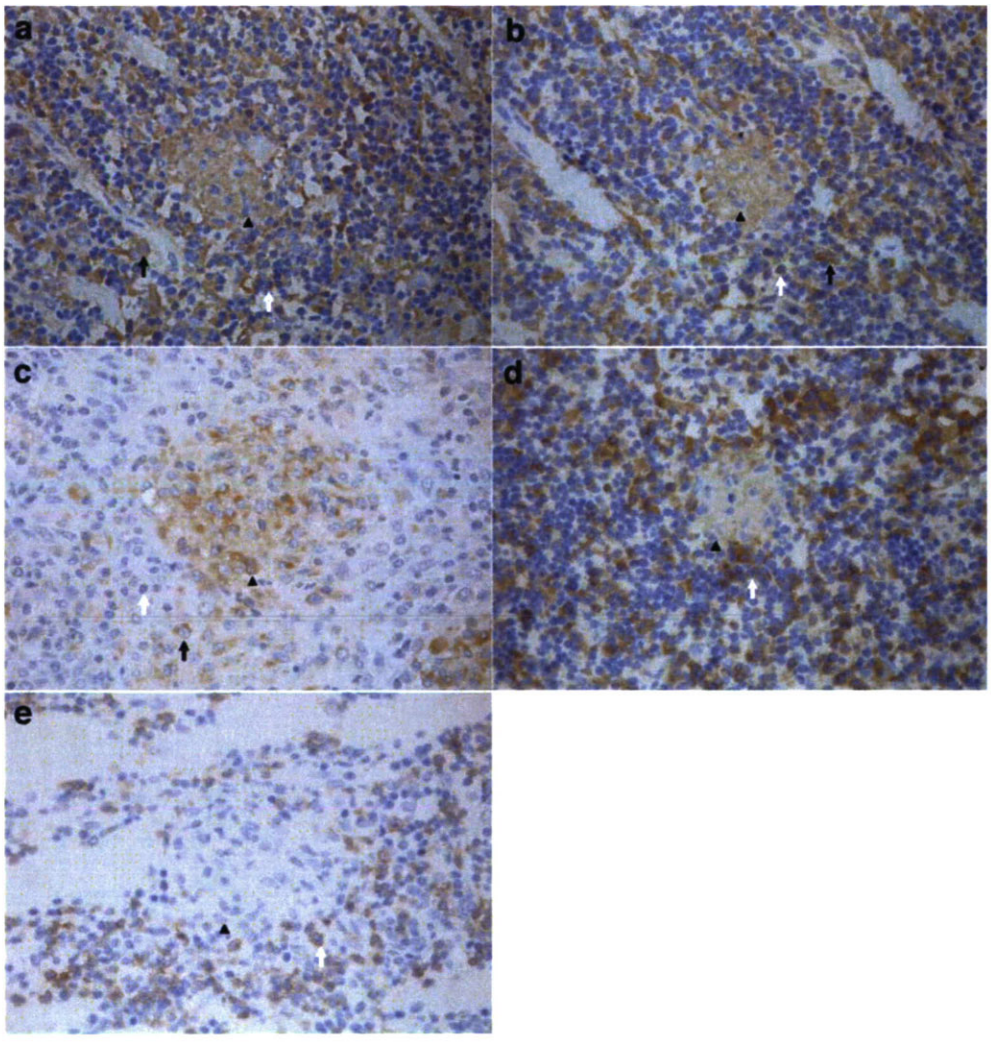

Fig. 2 Microscopic images (x 400) of immunostained for Ia antigen with MRC OX-3 (**a**), MRC OX-17 mAbs (**b**), and cell type characterization (**c-e**) in granulomas of control rats. **a** Accumulation of Ia+ epithelioid cells, Ia+ macrophages and Ia+ lymphocytes were characterized by MRC OX-3 mAb. **b** Accumulation of Ia+ epithelioid cells, Ia+ macrophages, and Ia+ lymphocytes were characterized by MRC OX-17 mAb. **c** The epithelioid cells and macrophages were determined by RM-4 positive staining. **d** CD4+ T cells (helper T cells) were determined by MRC OX-35 mAb. **e** CD8+ T cells (nonhelper T cells) were determined by MRC OX-8 mAb. *Black arrow head* indicates epithelioid cell granuloma; *black arrow*, macrophage infiltration; *white arrow*, lymphocyte infiltration

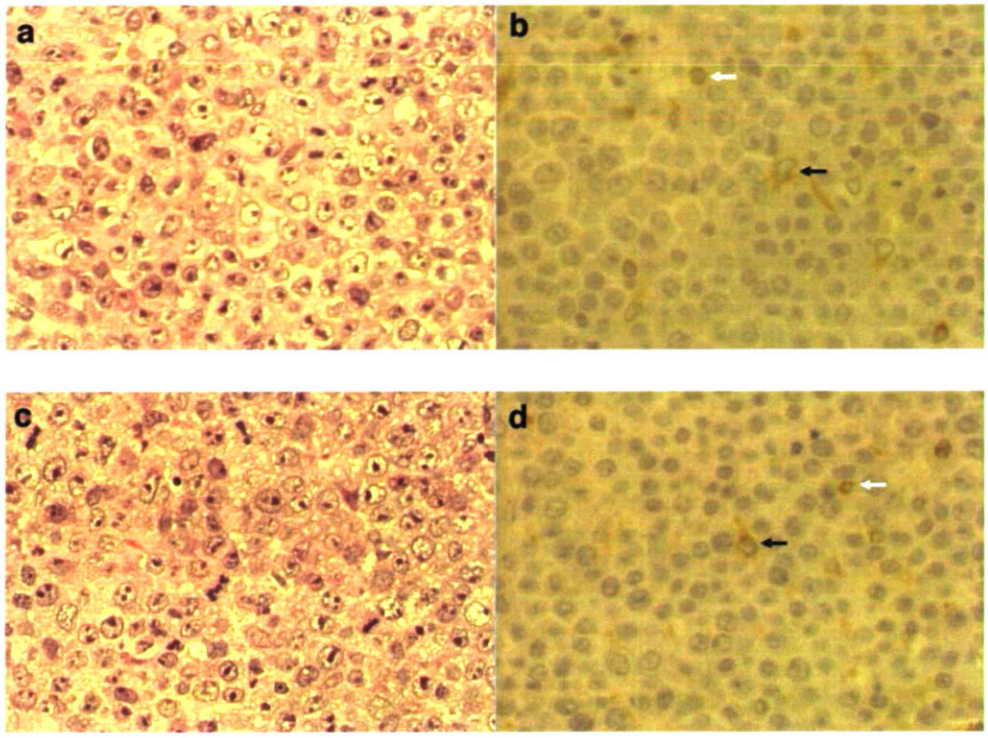

Fig. 3 Microscopic images (× 400) of HE-staining (**a**, **c**) and immunostaining with MRC OX-6 mAb for Ia antigen (**b**, **d**) in the control (**a**, **b**) and pretreated (**c**, **d**) rats bearing KDH-8 tumors. No pathological changes were observed in the tumor tissues between the untreated (control) and prednisolone-treated groups. *Black arrow* indicates macrophage infiltration; *white arrow*, lymphocyte infiltration

Uptake of FDG

FDG uptakes in the granuloma and tumor are summarized in Table 1 and Fig. 4. In the control groups, the level of FDG uptake in the granuloma was 0.909±0.142 (%ID/g) x kg which was comparable to that in the hepatoma (0.929× 0.164 (%ID/g) x kg). There was no significant difference in the level of FDG uptake between the granuloma and the tumor tissues (P=NS).

Prednisolone pretreatment significantly decreased the level of FDG uptake in the granuloma to 52% of the control value (P<0.001), while that in the tumor did not decrease significantly (85% of the control value; P=NS). The uptake levels of FDG in the granuloma and tumor tissues in the prednisolone pretreated group were 0.477± 0.139 and 0.788±0.080 (%ID/g) x kg, respectively, and the difference was significant (P<0.01) (Fig. 4).

The granuloma-to-muscle (L/M) and the granuloma-to-blood (L/B) ratios of FDG uptake were 33.5±9.7 and 9.4± 1.9 in the control group, respectively. Both the L/M ratio and L/B ratio of FDG uptake of the granuloma in the prednisolone pretreated group were significantly lower (14.4±4.0, P<0.01 for L/M ratio and 6.0±1.8, P<0.05 for L/B ratio) than those in the control group. Both the L/M ratio and L/B ratio of FDG uptake of the tumor were not significantly affected by the prednisolone pretreatment (Table 1).

Table 1 FDG uptake in granuloma and tumor

FDG uptake ((%ID/g) × kg)	Granuloma		Tumor	
	Control (n=5)	Steroid (n=6)	Control (n=6)	Steroid (n=5)
Granuloma or tumor	0.909±0.142	0.477±0.139**	0.929±0.164	0.788±0.080
Muscle	0.028±0.005	0.033±0.003	0.025±0.011	0.027±0.006
Blood	0.098±0.006	0.080±0.007**	0.060±0.017	0.054±0.015
L/M ratio	33.5±9.7	14.4±4.0**	41.0±10.9	29.6±6.0
L/B ratio	9.4±1.9	6.0±1.8*	15.9±2.4	15.3±3.2

L/M ratio, lesion (granuloma or tumor)-to-muscle ratio of FDG uptake
L/B ratio, lesion (granuloma or tumor)-to-blood ratio of FDG uptake
Control, control group; Steroid, prednisolone (PRE)-pretreated group
Data are mean±SD
*P<0.05, **P<0.01 compared with control group

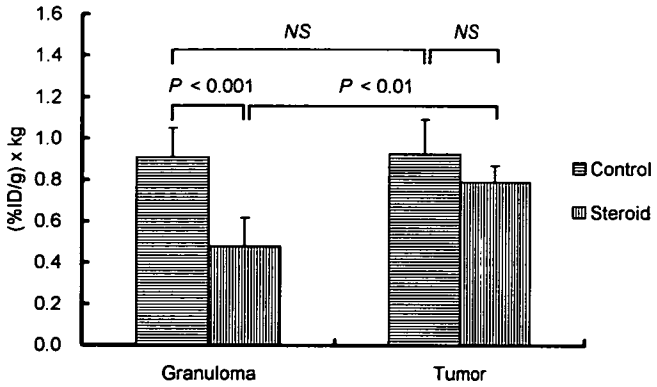

Fig. 4 FDG uptake in granuloma and tumor tissues in control and prednisolone pretreated groups. *Control* indicates the control group; *steroid* prednisolone (PRE)-pretreated group. *NS* is not statistically significant. Values given are mean ± SD

Blood glucose level and lesion weight

The blood glucose levels showed consistent tendency to increase by prednisolone pretreatment with a significant difference between the control and the pretreated rats bearing tumors (87.3±11.1 mg/dl vs 124.8±11.7 mg/dl at the time of FDG intravenous injection, $P<0.05$) (Table 2). The granuloma weight was significantly reduced by the prednisolone pretreatment (0.137±0.027 g for control rats and 0.089±0.024 g for pretreated rats, $P<0.05$), while the tumor weight was not (4.435±1.806 g for control rats and 4.085±2.083 g for pretreated rats, P=NS). There were no significant differences in the body weight of rats among all groups (Table 2).

PET images

Figure 5 shows representative FDG-PET images of rats bearing BCG granulomas or KDH-8 tumors before and after a prednisolone treatment. BCG granulomas and tumors were clearly visualized before the prednisolone treatment (Fig. 5a and c, control). Prednisolone treatment markedly reduced the uptake of FDG in BCG granulomas (Fig. 5b), but not in tumors (Fig. 5d).

Discussion

In this study, we developed an intramuscular granuloma rat model characterized by epithelioid cell granuloma-formation and massive lymphocyte-infiltration around the granuloma (Fig. 1a and b), histologically similar to those observed in sarcoidosis [11]. The granuloma showed high FDG uptake comparable to that of the tumor (Figs. 4 and 5). In addition, the present study demonstrated that the effect of prednisolone pretreatment on FDG uptake was greater in the granulomatous lesions than that in the tumor (Figs. 4 and 5). These results suggest that BCG-induced granuloma may be a valuable model and may provide a biological basis for FDG studies.

In our model, extensive FDG uptake was observed in the granuloma, which was comparable to that in the tumor. To the best of our knowledge, there have been no studies showing a comparison of FDG uptake in experimental granulomas and tumors, although increased FDG uptake in inflammatory lesions has been reported in experimental inflammation induced by an intramuscular injection of *S. aureus* or turpentine oil [5, 6]. In our previous study, the inflammatory lesions induced by *S. aureus* and turpentine oil showed levels of FDG uptake which were about 45% and 34% of that in KDH-8 tumor, respectively [6]. van Waarde et al. also suggested that FDG uptake in the turpentine oil-induced inflammatory lesion was about 35% of that in C6 rat glioma [5]. *S. aureus* and turpentine-induced inflammatory tissues showed massive neutrophil-infiltration and ambient connective tissue-formation around the injection sites of *S. aureus* and turpentine oil. Increased FDG distribution was mainly shown in the areas of neutrophil-infiltration, and FDG distribution was lower in the ambient connective tissues. On the contrary, in our granuloma model, increased FDG distribution was mainly shown in the epithelioid cell granulomas by our preliminary experiments using autoradiography (data not shown). The activities of granuloma formation and granuloma-associated immune cells may be reflected by FDG accumulation, although detailed mechanisms of the accumulation occur-

Table 2 Blood glucose level and body and lesions weights

		Granuloma		Tumor	
	Parameter	Control (n=5)	Steroid (n=6)	Control (n=6)	Steroid (n=5)
Blood glucose (mg/dl)	0 min	87.0±9.3	95.7±8.3	87.3±11.1	124.8±11.7*
	60 min	79.6±6.6	87.0±10.0	86.7±8.8	96.8±11.4
	Body weight (kg)	0.270±0.015	0.260±0.013	0.235±0.030	0.239±0.029
	Lesion weight (g)	0.137±0.027	0.089±0.024*	4.435±1.806	4.085±2.083

0 min at FDG injection; 60 min at sacrifice; Control indicates the control group; steroid, the prednisolone (PRE)-pretreated group
Data are mean ± SD
*$P<0.05$ compared with control group

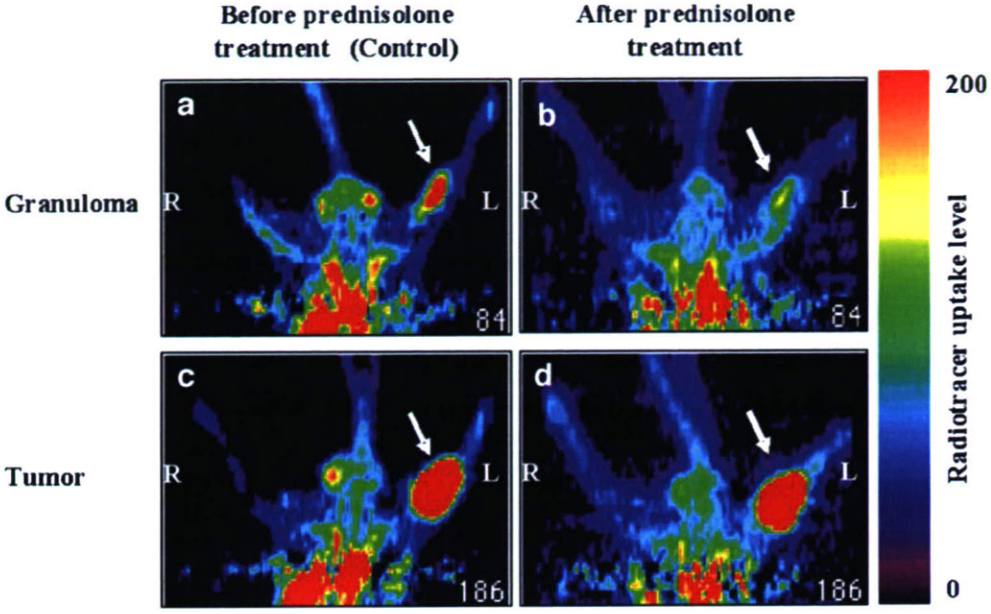

Fig. 5 FDG-PET images of rats bearing BCG granulomas (**a** and **b**) or KDH-8 tumors (**c** and **d**). Horizontal PET images before (**a** and **c**) and after prednisolone treatment (**b** and **d**) are shown. *Arrows* indicate the locations of BCG granulomas (**a** and **b**) and KDH-8 tumors (**c** and **d**) inoculated in the left calf muscles of rats. Color scale depicts radiotracer uptake level normalized to animal body weight and injected dose. *R* indicates right; *L*, left

ring in the granuloma remain unclarified. The animal models of inflammation induced by *S. aureus* and turpentine oil may not be suitable models for differentiating malignant tumors from benign diseases because of the relatively low FDG uptake levels in their inflammatory lesions. In contrast, our granuloma rat model showed a high FDG uptake in the granulomatous lesions comparable to that in the KDH-8 tumor, indicating the suitability of our model for such studies.

Our intramuscular granuloma rat model showed histologically similar characteristics to sarcoidosis [11, 12], as shown in Figs. 1 and 2. Sarcoidosis is a main source of false-positive FDG-PET findings in oncology. Sarcoidosis can be characterized in the affected organs by an accumulation of activated macrophages (epithelioid cells and multinuclear giant cells) and activated T lymphocytes at the site of disease activity. Pathologically, the first manifestation of the disease is an accumulation of mononuclear inflammatory cells, mainly CD4+ T helper 1 lymphocytes and mononuclear phagocytes in the affected organ. This inflammatory process is followed by the formation of granulomas, and aggregations of macrophages and their progeny, epithelioid cells, and multinucleated giant cells [13, 14]. This study showed the accumulation of epithelioid cells and macrophages defined by positive staining with RM-4 (Fig. 2c) in the granuloma, and CD4+ lymphocytes into the periphery of the granuloma (Fig. 2d), indicating the histological similarity of our model to sarcoidosis [9]. The cellular uptake of FDG in sarcoidosis is considered to be related to its inflammatory cell infiltrates, which are composed of lymphocytes, macrophages, and epithelioid cells from monocytes, because FDG has been observed in vitro to be accumulated by leukocytes [15, 16], lymphocytes, and macrophages [17]. The histological similarity of our granuloma rat model to sarcoidosis indicates its potential for providing a biological basis for differentiating sarcoidosis from malignant tumors, although detailed investigations, including those on FDG distribution at the cellular level, are required.

The immune-associated (Ia) antigen represents a 23,000- and 30,000-dalton membrane glycoprotein complex. The Ia antigen is normally expressed on all B-lymphocytes and some monocytes, but not in large amounts on normal T cells unless they are activated by allogenic or mitogenic stimulation [18]. The expression of Ia antigen on T cells is a sign of T cell activation in active sarcoidosis [19]. The present study also showed the accumulation of Ia positive (Ia^+) epithelioid cells and macrophages in the granuloma and Ia^+ lymphocytes into the periphery of the granuloma (Figs. 1, 2a and b), which further support the histological similarity of our model to sarcoidosis [9]. The extensive FDG uptake in the granuloma was decreased by prednisolone pretreatment, being concordant with the reduction in epithelioid cell granuloma-formation and lymphocyte-infiltration, including the infiltrations of Ia^+ macrophages and Ia^+ lymphocytes (Figs. 1c and d, 4b). These results suggest that FDG uptake might reflect active granulomatous processes.

For almost four decades, oral corticosteroids have been the mainstay of treatment in pulmonary sarcoidosis [20, 21]. To elucidate the mechanism of glucocorticoid on the suppressive course of the reaction to granulomatous lung tissue in experimental pulmonary granulomas, Gemma et al. [8] have performed immunohistochemical staining of an Ia+ antigen at 1 and 2 days after high-dose prednisolone treatment. The results showed a remarkable reduction in the number of Ia+ macrophages and Ia+ lymphocytes in the granulomatous lung tissue after the treatment with prednis-

olone. These findings suggest that glucocorticoid may suppress the immunological activities of macrophages and T cells through their inhibitory effect on the differentiation of Ia+ macrophages and activated T cells, which may result in the diminishment of the pulmonary granulomatous reaction through the disorder of the macrophage-T cell interaction. In patients with pulmonary sarcoidosis, FDG uptake in the lung was decreased after high-dose steroid therapy concordant with the histologic activity in the lung [2, 3, 14]. The present study showed that prednisolone pretreatment significantly decreased the level of FDG uptake in the granuloma to 52% of the control value (Table 1, Fig. 4). Our histological findings showed that the Ia^+ macrophage-infiltration, epithelioid cell granuloma-formation, and activated T lymphocyte-infiltration in the granuloma were decreased by prednisolone pretreatment. The decreased FDG uptake in the granuloma by the steroid pretreatment may be ascribed to the reduced histologic activity, including epithelioid cell granuloma-formation and lymphocyte-infiltration. The current results are in accordance with those in patients with pulmonary sarcoidosis [2, 3, 19]. On the other hand, the level of FDG uptake and histological features of the tumor were not significantly affected by the prednisolone pretreatment. Taken together, corticosteroid pretreatment may provide a potential means for differentiating malignant tumors from granulomatous lesions in FDG-PET studies, although further studies in other animal models and in patients are needed to confirm the present results.

In this study, to generate experimental tumors, allogenic hepatoma cells (KDH-8) were inoculated into the left calf muscle of rats. The histopathological characterization of intramuscular tumor tissues showed massive viable and proliferating cancer cells by HE staining and few Ia+ macrophage-infiltration and Ia+ lymphocyte-infiltration defined by the MRC OX-6 mAb into viable tumor cells 14 days after the inoculation of KDH-8. However, the inflammatory cells could seldom be seen around the tumor graft by HE and immunohistochemical stains. Hashimoto et al. [22] have also reported that the lesion consisted of many viable tumor cells with few tumor-tissue infiltrating lymphocytes in the tumor and several granulocytes and macrophages at the center of the tumor bearing into the leg muscle of WKAH rats 14 days after inoculation of KDH-8. In the present study, FDG uptake level in the tumor was decreased slightly after prednisolone treatment, although the difference was not significant (85% of the control value). On the other hand, there were no obvious histopathological changes in the tumor tissue after prednisolone treatment (Fig. 3c and d). Accordingly, the anti-inflammatory/immune effects of prednisolone may not be responsible for the reduction in tumoral FDG uptake level. Elevated blood glucose levels induced by corticosteroid and the antitumoral effects of prednisolone may be other explanations for the reduction in the tumoral FDG uptake level.

In the present study, the blood glucose levels showed consistent tendency to increase by the prednisolone pretreatment with a significant difference between the control and pretreated rats bearing tumor. It is well known that the action of steroids on glucose metabolism increases the blood glucose level [23, 24]. The uptake of FDG in tissues is affected by the blood glucose level [25, 26]. Accordingly, the reduced FDG uptake in the granuloma and tumor may be partly ascribed to the elevated blood glucose levels. However, the effect of prednisolone pretreatment on FDG uptake was greater in the granuloma than in the tumor, although the elevation in the blood glucose level was higher in rats bearing tumor. A slight elevation in the blood glucose level (125 mg/dl) following PRE pretreatment may not affect the uptake levels of FDG in the tumor, as reported previously [5, 27]. Detailed investigations, including quantitative evaluation of inflammation levels (i.e., determination of inflammatory cell density) and autoradiographic studies using FDG, are required to clarify the reason for the reduction in tumoral FDG uptake level.

As mentioned above, it is of great importance to clarify the detailed FDG distribution at the cellular level in the granuloma. In this regard, Kubota et al. reported a high FDG accumulation in young granulation tissues around the tumor and in the macrophages infiltrating the marginal areas surrounding the extensive tumor necrosis by micro-autoradiographies of FDG and ^{3}H-DG [17]. Activated inflammatory cells have markedly increased glycolysis. The hexose monophosphate shunt is stimulated by phagocytosis, which is enhanced 20–30-fold that of baseline values which is the cause of the high FDG uptake [28]. Although microautoradiographic studies of ^{3}H-FDG or ^{14}C-FDG are needed to clarify the detailed FDG distribution at the cellular level in our granuloma rat model, the results of this study indicate that a high FDG uptake in the granuloma is related to the activation of inflammatory cell infiltrates, including mature epithelioid cells, massive macrophages, and lymphocytes.

The PET images showed that BCG granuloma and tumors were clearly visualized before the prednisolone treatment (Fig. 5a and c, control). Prednisolone treatment markedly reduced FDG uptake in BCG granulomas but not in tumors (Fig. 5b and d). These results demonstrate that PET is a useful noninvasive imaging method to depict and assess early changes in FDG uptake by the corticosteroid treatment.

Low-grade hepatocellular carcinoma (HCC) has a low FDG uptake level due to its histological characteristics of being closer to the normal liver, which has abundant glucose-6-phophatase. However, high-grade HCC, intra-

and extrahepatic metastases, and distant metastases correlated with positivity of FDG-PET. Thus, FDG-PET imaging has a clinically significant impact on the management of patients diagnosed with HCC [29]. KDH-8 is a rat transplantable hepatocellular carcinoma that is found in WKAH rats and is histologically poorly undifferentiated. Our previous study showed that the FDG uptake level in the hepatoma was the same as or higher than that in the other tumor models [5]. Our hepatoma model, employed as an extrahepatic metastase, should provide a biological basis for evaluating the impact of FDG imaging on the management of patients diagnosed with hepatocellular carcinoma.

It should be noted that there are several limitations to our study. First, each rat was inoculated with BCG granulomas or KDH-8 tumors in this study because FDG uptake may be affected if both the BCG granulomas and the KDH-8 tumors were inoculated into the same rat. However, it is possible to inject BCG and KDH-8 cells in the same animal, and a rat model bearing both the BCG granulomas and the KDH-8 tumors may be useful to determine the differences in FDG uptake profiles between the granulomas and tumors. Second, anesthesia may affect FDG uptake, as the rats were kept under pentobarbital anesthesia during FDG uptake. In this regard, Lee et al. have reported that pentobarbital injection elevated blood FDG activity to 2.0-fold higher than the control levels, but had no effect on tumor uptake [30]. Recently, we compared the effects of pentobarbital and ketamine/medetomidine on FDG uptake in a rat model bearing KDH-8 tumors. The results showed no change in FDG uptake levels for either anesthetic agent. The effects of anesthesia on FDG uptake in tumors appeared to be small, compared with those in the brain. Finally, it is important to quantify the level of inflammation for FDG uptake correlation studies. Unfortunately, we could not perform quantitative evaluation of inflammation levels, which prevented us to accurately evaluate the correlation between the level of inflammation and FDG uptake level in the tumors and granulomas. Although our findings show that the pathological characterization of the BCG granulomas was similar to that of sarcoidosis, and FDG accumulation level was decreased by steroid treatment, detailed investigations, including quantitative evaluation of inflammation levels (i.e., determination of inflammatory cell density) and autoradiographic studies using FDG, are required to accurately evaluate the correlation between the level of inflammation and FDG distribution.

Conclusion

In the present study, we developed a BCG-induced granuloma rat model which has similar histopathological features as those of sarcoidosis. The granuloma showed a high FDG uptake comparable to that of the tumor. In addition, our results demonstrate that the effect of prednisolone pretreatment on FDG uptake was greater in the granuloma than in the tumor. These results suggest the usefulness of our model for studying FDG accumulation in inflammatory lesions.

Acknowledgments This work was supported in part by a grant-in-aid for Scientific Research from the Japan Society for the Promotion of Science, by a grant-in-aid for Scientific Research from the Japanese Ministry of Education, Culture, Sports, Science and Technology, by Special Coordination Funds for Promoting Science and Technology provided by the Ministry of Education, Culture, Sports, Science and Technology, the Japanese Government, by a Grant-in-Aid for Cancer Research from the Ministry of Health and Welfare of Japan, and by a grant from the Rotary Yoneyama Memorial Foundation, Inc. The authors are grateful to the staff members of the Department of Nuclear Medicine, Central Institute of Isotope Science and Institute for Animal Experimentation, Hokkaido University and the Facility of Radiology, Hokkaido University Hospital, for supporting this study. We also thank Eriko Suzuki, secretary of the professor of the Department of Nuclear Medicine, Hokkaido University, for continuously supporting this study and Makoto Sato, SHI Accelerator Service Ltd., for FDG syntheses.

References

1. Dimitrakopoulou-Strauss A, Strauss LG, Heichel T, Wu H, Burger C, Bernd L, et al. The role of quantitative (18)F-FDG PET studies for the differentiation of malignant and benign bone lesions. J Nucl Med 2002;43:510–8.
2. Brudin LH, Valind S, Rhodes CG, Pantin CF, Sweatman M, Jones T, et al. Fluorine-18 deoxyglucose uptake in sarcoidosis measured with positron emission tomography. Eur J Nucl Med 1994;21:297–305.
3. Lewis PJ, Salama A. Uptake of fluorine-18-fluorodeoxyglucose in sarcoidosis. J Nucl Med 1994;35:1647–9.
4. Ohtsuka T, Nomori H, Watanabe K, Naruke T, Orikasa H, Yamazaki K, et al. False-positive findings on [18F]FDG-PET caused by non-neoplastic cellular elements after neoadjuvant chemoradiotherapy for non-small cell lung cancer. Jpn J Clin Oncol 2005;35:271–3.
5. van Waarde A, Cobben DC, Suurmeijer AJ, Maas B, Vaalburg W, de Vries EF, et al. Selectivity of 18F-FLT and FDG for differentiating tumor from inflammation in a rodent model. J Nucl Med 2004;45:695–700.
6. Zhao S, Kuge Y, Tsukamoto E, Mochizuki T, Kato T, Hikosaka K, et al. Effects of insulin and glucose loading on FDG uptake in experimental malignant tumours and inflammatory lesions. Eur J Nucl Med 2001;28:730–5.
7. Zhao S, Kuge Y, Mochizuki T, Takahashi T, Nakada K, Sato M, et al. Biologic correlates of intratumoral heterogeneity in FDG distribution with regional expression of glucose transporters and hexokinase-II in experimental tumor. J Nucl Med 2005;46:675–82.
8. Gemma H, Sato A. Effect of glucocorticoid on lung tissue and bronchus-associated lymphoid tissue of experimental granulomatous lung. Kekkaku 1989;64:387–99.
9. Whiteland JL, Nicholls SM, Shimeld C, Easty DL, Williams NA, Hill TJ. Immunohistochemical detection of T-cell subsets

and other leukocytes in paraffin-embedded rat and mouse tissues with monoclonal antibodies. J Histochem Cytochem 1995;43: 313–20.
10. Watanabe M, Okada H, Shimizu K, Omura T, Yoshikawa E, Kosugi T, et al. A high resolution animal PET scanner using compact PS-PMT detectors. IEEE Trans Nucl Sci 1997;44:1277–82.
11. Schrier DJ, Ripani LM, Katzenstein AL, Moore VL. Role of angiotensin-converting enzyme in bacille Calmette-Guerin-induced granulomatous inflammation. Increased angiotensin-converting enzyme levels in lung lavage and suppression of inflammation with captopril. J Clin Invest 1982;69:651–7.
12. Sandor M, Weinstock JV, Wynn TA. Granulomas in schistosome and mycobacterial infections: a model of local immune responses. Trends Immunol 2003;24:44–52.
13. Chang JM, Lee HJ, Goo JM, Lee HY, Lee JJ, Chung JK, et al. False positive and false negative FDG-PET scans in various thoracic diseases. Korean J Radiol 2006;7:57–69.
14. du Bois RM. Corticosteroids in sarcoidosis: friend or foe? Eur Respir J 1994;7:1203–9.
15. Osman S, Danpure HJ. The use of 2-[18F]fluoro-2-deoxy-D-glucose as a potential in vitro agent for labeling human granulocytes for clinical studies by positron emission tomography. Int J Rad Appl Instrum B 1992;19:183–90.
16. Borregaard N, Herlin T. Energy metabolism of human neutrophils during phagocytosis. J Clin Invest 1982;70:550–7.
17. Kubota R, Yamada S, Kubota K, Ishiwata K, Tamahashi N, Ido T. Intratumoral distribution of fluorine-18-fluorodeoxyglucose in vivo: high accumulation in macrophages and granulation tissues studied by microautoradiography. J Nucl Med 1992;33:1972–80.
18. Winchester RJ, Kunkel HG. The human Ia system. Adv Immunol 1979;28:221–92.
19. Costabel U, Bross KJ, Ruhle KH, Lohr GW, Matthys H. Ia-like antigens on T-cells and their subpopulations in pulmonary sarcoidosis and in hypersensitivity pneumonitis. Analysis of bronchoalveolar and blood lymphocytes. Am Rev Respir Dis 1985;131:337–42.
20. Siltzbach LE. Effects of cortisone in sarcoidosis: a study of thirteen patients. Am J Med 1952;12:139–60.
21. Milman N. Oral and inhaled corticosteroids in the treatment of pulmonary sarcoidosis—a critical reappraisal. Sarcoidosis Vasc Diffuse Lung Dis 1998;15:150–7.
22. Hashimoto S, Shirato H, Hosokawa M, Nishioka T, Kuramitsu Y, Matushita K, et al. The suppression of metastases and the change in host immune response after low-dose total-body irradiation in tumor-bearing rats. Radiat Res 1999;151:717–24.
23. West KM. Comparison of the hyperglycemic effects of glucocorticoids in human beings; the effect of heredity on responses to glucocorticoids. Diabetes 1957;6:168–75.
24. Pellacani A, Fornengo P, Bruno A, Ceruti C, Mioletti S, Curto M, et al. Acute methylprednisolone administration induces a transient alteration of glucose tolerance and pyruvate dehydrogenase in humans. Eur J Clin Invest 1999;29:861–7.
25. Wahl RL, Henry CA, Ethier SP. Serum glucose: effects on tumor and normal tissue accumulation of 2-[F-18]-fluoro-2-deoxy-D-glucose in rodents with mammary carcinoma. Radiology 1992;183:643–7.
26. Lindholm P, Minn H, Leskinen-Kallio S, Bergman J, Ruotsalainen U, Joensuu H. Influence of the blood glucose concentration on FDG uptake in cancer—a PET study. J Nucl Med 1993;34:1–6.
27. Zhao S, Kuge Y, Nakada K, Mochizuki T, Takei T, Okada F, et al. Effect of steroids on [18F]fluorodeoxyglucose uptake in an experimental tumour model. Nucl Med Commun 2004;25:727–30.
28. Amrein PC, Larson SM, Wagner HN Jr. An automated system for measurement of leukocyte metabolism. J Nucl Med 1974; 15:352–5.
29. Wudel LJ Jr, Delbeke D, Morris D, Rice M, Washington MK, Shyr Y, et al. The role of [18F]fluorodeoxyglucose positron emission tomography imaging in the evaluation of hepatocellular carcinoma. Am Surg 2003; 69:117–24.
30. Lee KH, Ko BH, Paik JY, Jung KH, Choe YS, Choi Y, et. al. Effects of anesthetic agents and fasting duration on 18F-FDG biodistribution and insulin levels in tumor-bearing mice. J Nucl Med 2005;46:1531–6.

Invited Review Article

Chemical Control of Biological Activity and Biodistribution of Metal Compounds : Drug Design of Metal Complexes with Biological Activity and Target-Specific Biodistribution

Hideo Saji[1], Kazuma Ogawa[2], Youji Kitamura[3], Megumi Kubota-Akizawa[1] and Hidekazu Kawashima[1]

[1] Department of Patho-functional Bioanalysis, Graduate School of Pharmaceutical Sciences, Kyoto University, Kyoto 606-8501, Japan
[2] Central Institute of Radioisotopes Science, Division of Tracer Kinetics, Advanced Science Research Center, Kanazawa University, Kanazawa 920-8640, Japan
[3] Graduate School of Medicine and Dentistry and Pharmaceutical Sciences, Okayama University, Okayama 700-8558, Japan

Abstract

The development of metallic compounds for the diagnosis and therapy of diseases has been expected to open a new field of medicinal science. These compounds are required to exhibit biological activity and a specific localization to the target tissue. These demands constitute a great challenge on the rational design of metallic compounds and we have proposed two approaches, a pendant approach and an integrated approach in order to achieve this purpose. The pendant approach involves designing a biologically active compound by the attachment of a chelating group for binding the metal ion to a mother compound without the effect on the inherent biospecificity of the mother compound. A typical example of the pendant approach is bifunctional radiopharmaceuticals used for nuclear medical diagnosis and internal radiotherapy. The integrated approach involves designing a metallic compound with a biologically activity and physicochemical properties suitable for target-specific delivery by coordination to a mother compound with metal ion.

This review will describe our recent progress in research on a bifunctional radiopharamceutical labeled with metallic radionuclides, Rhenium-186 for therapy of painful bone metastases as an example of the pendant approach and a lipophilic zinc complex with protective effect against ischemic neuronal injury as an example of the integrated approach.

Keywords : metallic compound, drug design, bifunctional radiopharmaceutical, rhenium-186, bisphosphonates, zinc, neuroprotection.

1. Introduction

Many metallic compounds have biological activities, but the application of these compounds in the medical field has been limited. The development of metallic compounds for the diagnosis and treatment of diseases has been expected to open a new field of medicinal science. However, metallic compounds are required to exhibit biologically appropriate activity and a specific localization to target tissue. To obtain such compounds, we have proposed two approaches, a pendant approach and an integrated approach (Fig. 1).

The pendant approach involves designing a compound containing independent groups both with the ability to deliver into the targeted tissue/organ and with the ability to bind metallic ions. In the pendant approach, compounds with a radiometallic nuclide for nuclear medical diagnosis and internal radiotherapy, called "bifunctional

Address correspondence to :
Hideo Saji, Ph.D.
Department of Patho-Functional Bioanalysis, Graduate School of Pharmaceutical Sciences, Kyoto University, Yoshida Shimoadachi-cho, Sakyo-ku, Kyoto 606-8501, Japan
TEL : +81-75-753-4556
FAX : +81-75-753-4568
E-mail : hsaji@pharm.kyoto-u.ac.jp

Received : 20 October 2006
Accepted : 2 March 2007

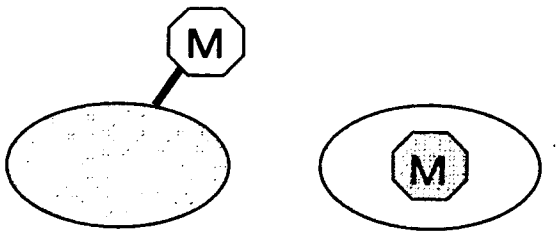

Fig. 1 Concept of the pendant approach and integrated approach.

radiopharmaceuticals", are of particular interest [1-3].

The integrated approach involves designing metallic compounds with physicochemical properties suitable for targeted delivery. A typical example is the development of a lipophilic metallic compound for improving the ability to penetrate the blood-brain barrier [4-6]. Another example is raising the water-solubility to prompt renal excretion.

This review will describe recent progress in our research into bifunctional radiopharmaceuticals labeled with metallic radionuclides for therapy as an example of the pendant approach and a lipophilic zinc complex with a protective effect against ischemic neuronal injury as an example of the integrated approach.

2. Pendant approach

2.1 Concept of the pendant approach : Bifunctional radiopharmaceutical

Nuclear medicine is a diagnostic tool used to visualize changes in physiological and biochemical processes throughout living tissues and organs as well as in regional anatomy (Fig. 2). Furthermore, nuclear medicine has applications to therapy, based on the radiation of radioactive nuclides. Drugs containing radioactive nuclides to be used in nuclear medicine are called radiopharmaceuticals. Radiopharmaceuticals are required to have certain biological properties : a high level of radioactivity localized to the target tissue and a high target/non-target tissue ratio for clear imaging or effective therapy.

The radioactive nuclides used in diagnostic nuclear medicine are short-lived, low gamma energy emitters. In internal radiotherapy, beta- or alpha particle emitters, which provide high radiation doses, are useful as therapeutic radionuclides. The radionuclides used for these purposes include some radioisotopes of metallic elements. Thus, the great demand for biospecific metallic radiopharamceuticals has evolved into the rational design of so called "bifunctional radiopharmaceuticals" ; that is, a radiopharmaceutical containing a group for the selective targeting of diseased tissue together with a group with the ability to bind radiometallic nuclides [1-3] (Fig. 3). Research on bifunctional radiopharmaceuticals started with the development of radiolabeled macromolecules, such as proteins [1,7,8]. In recent years, bifunctional radiopharmaceuticals have also been used for the labeling of non-protein compounds such as peptides and drugs of low molecular weight [1,9,10].

The pendant approach involves hanging the metal complexing moiety from the main body of the molecule responsible for delivery to the target site. The key to this design for small molecules is the strategic placement of the radiometal-chelate-tether moiety at a site on the ligand toward which the molecule responsible for biological function is sterically tolerant.

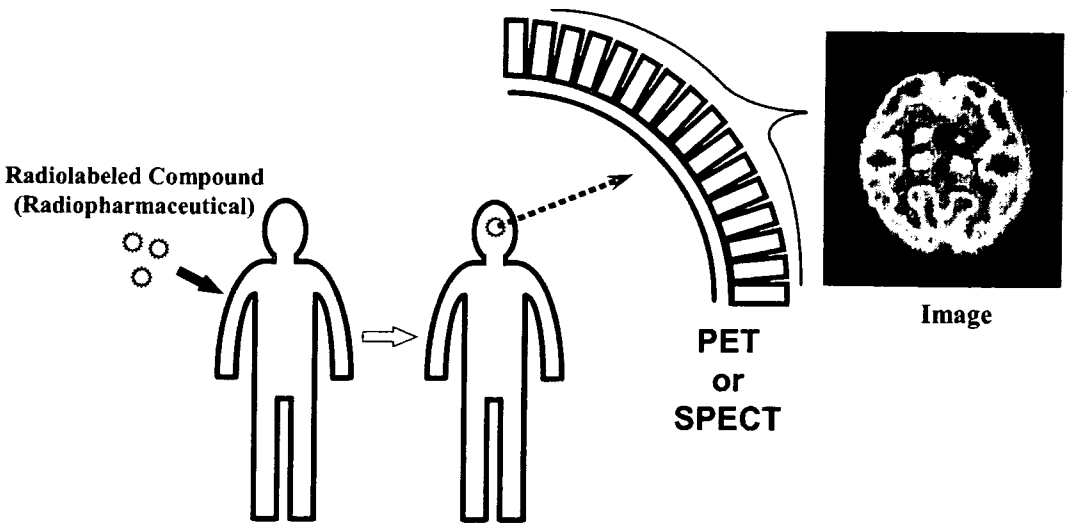

Fig. 2 Targeted imaging system (diagnostic nuclear medicine)

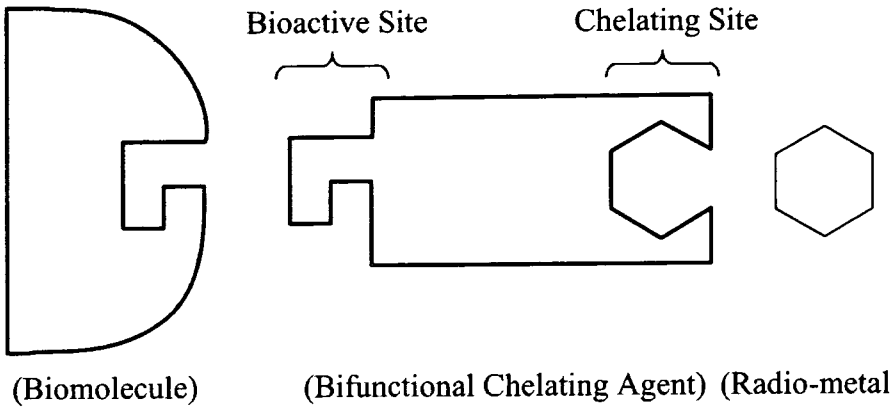

Fig. 3 Bifunctional radiopharmaceutical.
A molecule holding two reactive sites for binding the biomolecule and chelating the radiometal is called a bifunctional chelating agent.

2.2 Development of Rhenium-186-chelate-conjugated Bisphosphonates for painful bone metastases

Malignant tumors frequently metastasize to the bone. A prominent symptom of these metastases is pain, which affects the patient's quality of life, and is an important clinical problem [11]. Localized radiation therapy is an effective modality for localized lesions, providing palliation of bone pain, however, a common problem in patients with bone metastases is the development of multiple sites of metastasis, and so internal radiotherapy using specifically localized beta emitters is preferable [12]. Recently, $^{89}SrCl_2$ has been used as a palliative agent for painful osseous metastases. However, ^{89}Sr is a pure beta emitter and has a relatively long half-life (50.5 d). These physical properties could be a disadvantage for clinical use. The use of Rhemium-186-1-hydroxyethylidene-1,1-diphosphonate (^{186}Re-HEDP) has also been proposed for the palliation of metastatic bone pain [13]. ^{186}Re is a promising radionuclide with a maximum beta emission of 1.07 MeV and gamma ray emission of 137 keV (9%), making it adequate for therapy and imaging, respectively. Furthermore, the physical half-life of ^{186}Re is 3.8 days, which is adequate for shipment and processing of the radiopharmaceutical but not too long for the disposal of radioactive waste. However, it has reported that ^{186}Re-HEDP shows a delayed blood clearance and high gastric uptake due to the poor stability of the ^{186}Re complex in vivo leading to the generation of ^{186}Re-perrhenate ($^{186}ReO_4^-$) [14,15]. Furthermore, though the accumulation in bone as a definitive factor of therapeutic effect is more important, the instability of ^{186}Re-HEDP described above may decrease the bone uptake.

Thus, based on the idea of bifunctional radiopharmaceuticals, we developed a novel ^{186}Re-chelate-conjugated bisphosphonate (^{186}Re-MAMA-BP, Fig. 4-A), introducing a highly stable ^{186}Re-MAMA complex to improve the instability of ^{186}Re-HEDP [16].

To evaluate the stability of ^{186}Re complexes in vitro, ^{186}Re-MAMA-BP and ^{186}Re-HEDP were incubated in phosphate-buffered saline. After 24 hours of incubation, about 80% of the ^{186}Re-MAMA-BP remained intact, compared to only about 30% of the ^{186}Re-HEDP. This is because the ^{186}Re-HEDP was degraded to $^{186}ReO_4^-$ with time. In biodistribution experiments in mice, ^{186}Re-MAMA-BP showed a significantly lower uptake by the stomach than ^{186}Re-HEDP. Since ReO_4^- is known to accumulate in the stomach, accumulation in the stomach is an index of the decomposition of a Re-complex in biodistribution studies. Then, a lower level of ^{186}Re-MAMA-

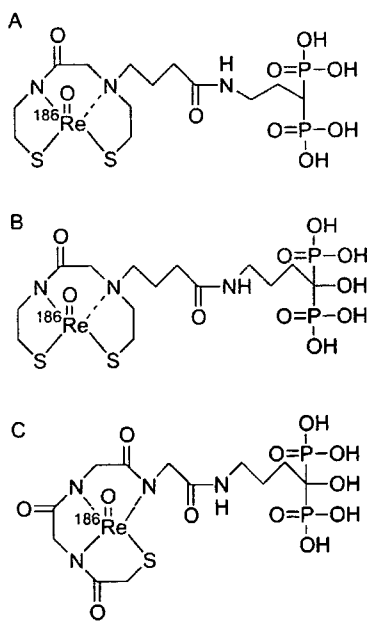

Fig. 4 Structures of ^{186}Re-MAMA-BP (A), ^{186}Re-MAMA-HBP (B), and ^{186}Re-MAG3-HBP (C).

BP in the stomach indicates better stability in vivo.

Meanwhile, ^{186}Re-MAMA-BP showed a faster clearance from the blood than did ^{186}Re-HEDP (Fig. 5-A). It was reported that the ^{186}Re-HEDP complex gave rise to $^{186}ReO_4^-$ in vivo and the clearance from blood of $^{186}ReO_4^-$ was slower than that of ^{186}Re-HEDP. It is suggested that the more rapid clearance from the blood of ^{186}Re-MAMA -BP is responsible for its stability, when compared with ^{186}Re-HEDP. Furthermore, ^{186}Re-MAMA-BP showed a rapid accumulation and long residence in the bone, and its uptake by the bone was significantly greater than that of ^{186}Re-HEDP (Fig. 5-B). The better accumulation of ^{186}Re-MAMA-BP in bone would be partly caused by its greater stability.

Bisphosphonates have been widely used as inhibitors of bone resorption for the treatment of bone diseases and extensively investigated [17]. All bisphosphonates contain two phosphonate groups attached to a single carbon atom, forming a P-C-P structure, and this central carbon has various side chains. It was reported that bisphosphonates containing a hydroxy group have higher affinity for bone mineral [18]. We supposed that the therapeutic effect of ^{186}Re complex-conjugated bisphosphonate could be increased by the introduction of a hydroxy group, then we developed ^{186}Re-MAMA-HBP (Fig. 5-B) [19]. To investigate the affinity for bone in vitro, a hydroxyapatite-binding assay was performed. As expected, ^{186}Re-MAMA-HBP showed a greater affinity for hydroxyapatite beads than did ^{186}Re-MAMA-BP (Fig. 6). This result was reflected by its behavior in vivo. In biodistribution experiments, more ^{186}Re-MAMA-HBP than ^{186}Re-MAMA-BP accumulated in bone. These findings suggest that a hydroxyl group at the central carbon in the design of ^{186}Re-chelate-conjugated bisphosphonates plays a critical role in the enhancement of bone accumulation.

^{186}Re-MAMA-HBP showed the desired properties, namely, greater accumulation in the bone and rapid clearance from the blood. However, hepatic radioactivity levels were significantly higher after the administration of ^{186}Re-MAMA-HBP and ^{186}Re-MAMA-BP than ^{186}Re-HEDP (Fig. 5-C), possibly caused by the increase in lipophilicity with the introduction of the ^{186}Re-MAMA complex into the bisphosphonate structure.

Thus, we developed a ^{186}Re-labeled MAG3-conjugated bisphosphonate (^{186}Re-MAG3-HBP, Fig. 4-C) to modify the physicochemical characteristics of ^{186}Re-MAMA-HBP and ^{186}Re-MAMA-BP and to reduce their hepatic uptake [20]. MAG3 was selected as the ^{186}Re-chelating group because it could form a stable and more hydrophilic complex with ^{186}Re.

^{186}Re-MAG3-HBP also showed good stability in buffered solution. After 24 hours of incubation, about 95% of ^{186}Re-MAG3-HBP remained intact. In biodistribution experiments, ^{186}Re-MAG3-HBP also showed a much higher accumulation in the bone and a faster clearance from the blood than did ^{186}Re-HEDP (Fig. 5-A,B). Furthermore, hepatic radioactivity levels were significantly lower after the administration of ^{186}Re-MAG3-HBP than of ^{186}Re-MAMA-HBP and ^{186}Re-MAMA-BP (Fig. 5-C). The results of the biodistribution experiments and partition coefficients (^{186}Re-MAMA-BP : -0.96±0.01, ^{186}Re-MAMA -HBP : -1.02±0.01, and ^{186}Re-MAG3-HBP : -2.68±0.01, respectively) indicated that the high hepatic uptake of ^{186}Re-MAMA-conjugated bisphosphonates was attributable to the physicochemical properties of the ^{186}Re-MAMA complex.

In summary, we developed highly stable ^{186}Re-chelate-conjugated bisphosphonates, ^{186}Re-MAMA-BP, ^{186}Re-MAMA-HBP, and ^{186}Re-MAG3-HBP. These agents showed higher bone : blood ratios of radioactivity in mice than did ^{186}Re-HEDP, resulting from greater accumulation in the bone and rapid clearance from the blood.

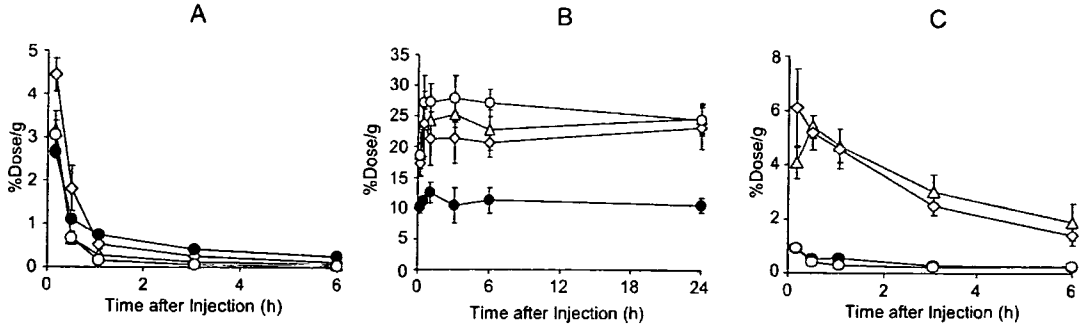

Fig. 5 Biodistribution (A : Blood, B : Bone, C : Liver) of ^{186}Re-MAMA-BP (open diamonds), ^{186}Re-MAMA-HBP (open triangles), ^{186}Re-MAG3-HBP (open circles), and ^{186}Re-HEDP (closed circles) in mice.

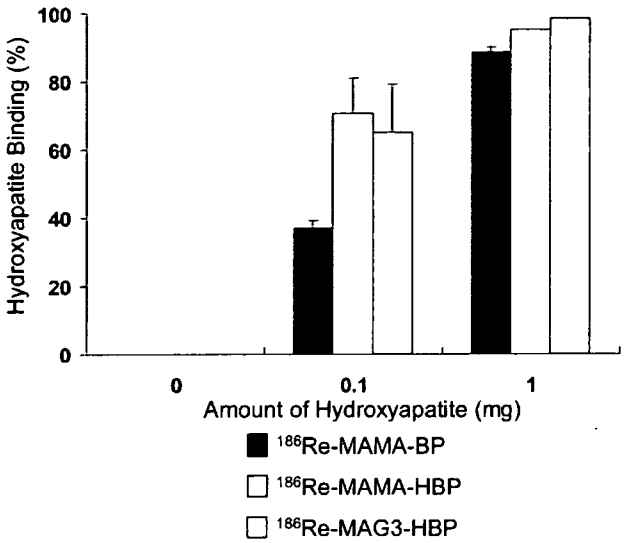

Fig. 6 Binding to hydroxyapatite of ^{186}Re-MAMA-BP, ^{186}Re-MAMA-HBP, and ^{186}Re-MAG3-HBP.

Among these ^{186}Re-chelate-conjugated bisphosphonates, ^{186}Re-MAG3-HBP showed a superior biodistribution as a bone-seeking agent because of its high selectivity for bone as a target tissue. The present findings would provide useful information on the drug design of bone-seeking therapeutic radiopharmaceuticals.

3. Integrated approach

3.1 Concept of integrated approach

The integrated approach involves the incorporation of a group containing physicochemical properties suitable for targeted delivery into a biologically active metal complex, resulting in both an improvement in biodistribution and the preservation of the biological activity of the metallic compound[1]. However, this design often results in a more synthetically challenging target molecule, and the challenge of maintaining biological activity is often greater as well.

2.2 Development of a highly membrane permeable zinc complex providing protection against ischemic neuronal injury.

2.2.1 Studies on the movement and effect of vesicular zinc in brain ischemia

The brain contains an abundant amount of zinc, particularly in the hippocampus, cerebral cortex, and limbic system[21]. About 10% of all zinc in the brain exists in the presynaptic vesicles of glutamatergic neurons and is released into synaptic clefts upon the excitation of nerves [22,23]. On the other hand, the influx of calcium through *N*-methyl-D-asparate (NMDA) receptors induced by glutamate, which is excessively released from glutamatergic nerve terminals into synaptic clefts during brain ischemia, is thought to relate with neuronal death after ischemia. In addition, some studies reported that zinc inhibits NMDA receptors by interacting with the zinc-binding site on the receptors [24]. These studies suggest that zinc, which is released from synaptic vesicles during brain ischemia along with glutamate, may exert a protective effect against glutamate-induced neuronal injury by blocking the influx of calcium via NMDA receptors. Conversely, many reports have indicated that an excessive amount of synaptic vesicular zinc is released during forebrain ischemia, and the released zinc might cause delayed neuronal death after ischemia [25]. Thus, there are conflicting reports about the effect of synaptic vesicular zinc on ischemic neuronal injury, and so the exact role of vesicular zinc is still unclear. One of the key points of this argument is the concentration of zinc released during ischemia, but there have been few reports that describe the effect of zinc based on its concentration directly determined *in vivo*. Therefore, we investigated the movement and effect of zinc in ischemia based on quantity *in vivo*.

First, the effect of various concentrations of zinc on glutamate-induced calcium influx and neuronal death were examined in cultured hippocampal neurons [26]. The addition of a low concentration (under 100 μM) of zinc inhibited both glutamate-induced calcium influx and neuronal death. In contrast, a higher concentration (over 150 μM) of zinc decreased neuronal viability although calcium influx was still inhibited, which means that a high concentration of zinc exerts its own neurotoxicity. These results indicate that zinc exhibits biphasic effects depending on its concentration. On the other hand, co-addition of glutamate and Ca-EDTA, which binds extracellular zinc, increased glutamate-induced calcium influx and aggravated the neurotoxicity of glutamate. These results suggest that, in cultured neurons, vesicular zinc was released by glutamate and the concentration released might be low, exhibiting a neuroprotective effect against the neurotoxicity of glutamate.

To investigate the movement and effect of vesicular zinc in a model of ischemia, we investigated the temporal change to extracellular zinc and glutamate levels in the cortex using microdialysis in rats with middle cerebral artery occlusion (MCAO) [27,28]. The microdialysis experiment revealed that the extracellular concentration of zinc in the cortex increased transiently reaching a peak 30 min after occlusion, then decreased with time, returning to the basal level after reperfusion (Fig. 7). This time

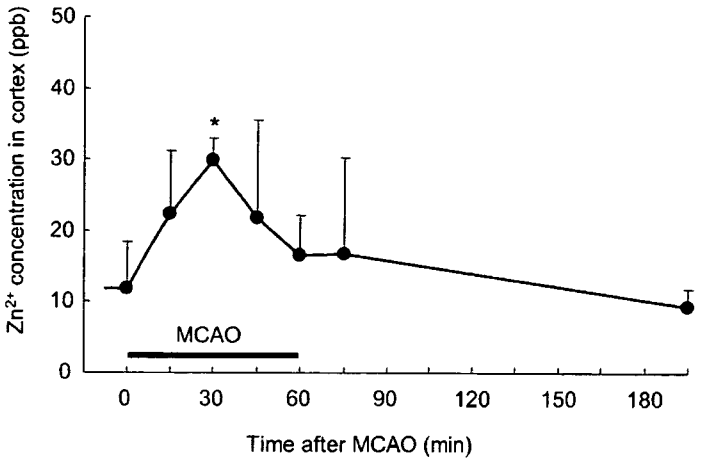

Fig. 7 Extracellular Zn^{2+} levels in the cortex during MCAO.
Data are expressed as the mean ± S.D. *p < 0.05 for significantly different from the pre-ischemic level (Dunnett's test).

course is consistent with that of glutamate. At the peak, the extracellular zinc concentration was about twice the basal level, in contrast with the amount of glutamate which increased about 50 fold. These results suggest that, the concentration of zinc released during MCAO could not reach a toxic level. In this model, intracerebroventricular (i.c.v.) injection of Ca-EDTA 30 min prior to occlusion, accelerated the increase of infarction volume (Fig. 8). N-(6-methoxy-8-quinolyl)-p-toluenesulfonamide (TSQ) staining revealed that there no zinc accumulated in the infarcted area or at its boundary. These results suggest that, in the rat MCAO model, the zinc released from synaptic vesicles may provide protection against ischemic neuronal injury. These results suggest that the effect of zinc on ischemic neuronal death differs depending on the ischemic region or severity.

2.2.2. Development of a highly membrane permeable zinc complex providing protection against ischemic neuronal injury

As shown in 2.2.1, Zn^{2+} blocks NMDA-induced depolarizing currents and protects cultured cortical neurons from the NMDA receptor-mediated neurotoxicity of glutamate. The results suggested the potential usefulness of zinc for the prevention of ischemic neuronal damage in the brain.

The basic requirements for therapeutic drugs to effectively prevent ischemic neuronal damage in the brain include high membrane permeability resulting in a rapid and significant uptake in the brain and protective action against glutamate's toxicity. However, Zn^{2+} does not readily permeate the blood brain barrier due to its high polarity [29]. Thus, a zinc compound that can cross cell

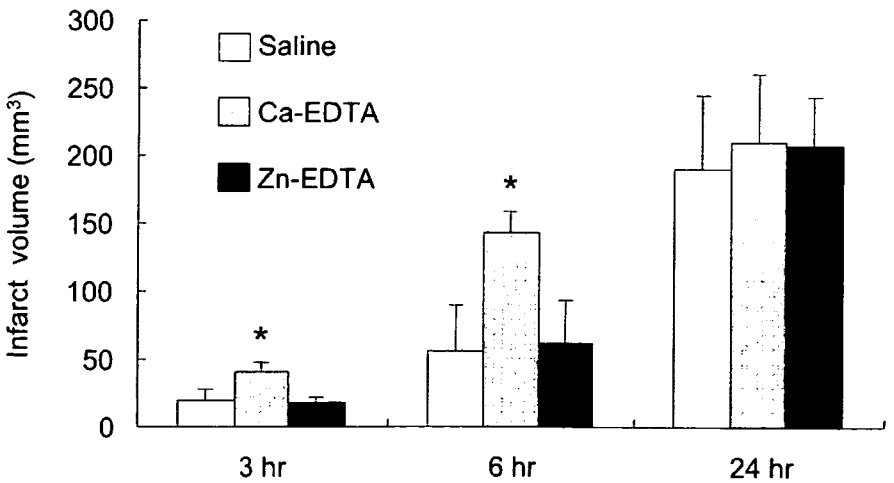

Fig. 8 Effect of Ca- and Zn-EDTA on the development of infarcted areas after MCAO.
Data are expressed as means ± S.D. (n= 3- 5). *P< 0.01 for significantly different from the saline-treated group (Dunnett's test).